Attitude determination of cylindrical rocket bodies by using simultaneous bistatic photometric measurements

Tomáš Hrobár, Jiří Šilha, Matej Zigo, Peter Jevčák
Faculty of Mathematics, Physics and Informatics, Comenius University, Bratislava, Slovakia
Palash Patole, Thomas Schildknecht
Astronomical Institute, University of Bern, Switzerland

ABSTRACT

The rocket bodies, as a part of the space debris population, poses a significant threat and are one of the prime targets for active debris removal (ADR) missions due to their large size and orbital regimes. Accurate monitoring of their dynamic properties like rotation period and tumbling axis is crucial for predicting their orientation and assisting potential applicable ADR missions.

We determine the tumbling axis direction using the low-resolution Williams model [1] based on our own photometric measurements. This model is ideal for cylindrical objects, assuming rotation around an axis perpendicular to the central axis in body-fixed reference frame. From the brightness ratio, which represents the difference between maximum and minimum brightness values during one rotation, it can estimated the possible tumbling axis orientation. The brightness ratio depends on the object's position, tumbling axis orientation, and observer's location. Typically, when both the observer's location and object's position are known, we can derive the brightness ratio from the series photometric measurements.

This method requires at least two observations from different perspectives over a relatively short period, as large changes in the tumbling axis are not expected by the model. Collecting data simultaneously from two different locations helps meet these challenges in the most effective way.

We present tumbling axis estimations for CZ-3B, H-2A and FALCON 9 rocket bodies, selected as calibration test objects. They are expected to rotate about an axis perpendicular to their central axis due to their moments of inertia. These objects mainly reflect light from their mantle, aligning well with the Williams model [1]. Our results are based on photometric measurements from two telescopes, AGO70 located in Slovakia and ZIMLAT located in Switzerland, focusing on CZ-3B, H-2A and FALCON 9 upper stages with eccentric orbits and low perigee distances, simulating near-future re-entries and close-range observations of LEO objects. This approach aims to establish a methodology applicable to LEO objects, as potential targets for future ADR missions.

1. INTRODUCTION

Monitoring of space debris population is important because of its threat to human space activities and also in case of re-entry for better assessment of the impact risk. The space debris population is becoming larger with every new launch. There are more than $30,000$ objects with diameters between $5-10$ *cm* and larger, and millions of objects from 1 *mm* to 1 *cm* with velocities up to 11.2 km/s. Such objects at these speeds, although sometimes with small dimensions, are very dangerous for active spacecraft and space stations. To stabilize the growth and to minimize the future creation of new debris objects, it is necessary to actively reduce the population. One option is to actively remove large compact objects, situated at highly populated regions, from their orbits with Active Debris Removal missions (ADR) or to increase the lifetime of satellites by performing In-Orbit Servicing (IOS). The knowledge of the axial rotation, tumbling axis direction and rotational period and physical processes affecting them is essential to clearly describe the behaviour of the objects and properly decide, whether an object could be removed or serviced.

Space debris has unique kinematic and dynamical properties, which are necessary to determine for each object. Debris objects are under the constant influence of various torques and forces: gravitational perturbations, Earth's magnetic

field variations, and torques depending on the object's physical properties such as the moment of inertia, the center of mass, area-to-mass ratio, complexity of the shape, conductivity, etc. Objects on low Earth orbits (LEO) or objects on eccentric orbits with low perigee distances, which are possible candidates for ADR, are under influence of all mentioned torques and also these are influenced by the non-gravitational perturbations caused by the upper parts of the atmosphere. Non-gravitational perturbations caused by the Sun are dominant for the objects on geostationary orbit (GEO) which are targets for current IOS missions.

Low resolution attitude determination Williams method [1] is suitable for the determination of tumbling axis orientation of the cylindrical objects. This approach necessitates observing the target with various perspectives i.e., phase angles. However, achieving this observing from only one location is not always feasible due to weather conditions or the object's observability. Furthermore, to resolve a more rapid change in the tumbling axis orientation necessitates both improved time resolution in the acquired photometric series and shorter intervals between data points to ensure a more precise sampling of attitude changes. One possible solution for addressing this condition involves conducting quasi-simultaneous observations from multiple observatories. This paper represents the initial summary of the observation campaign, which aimed to achieve two main goals:

- Demonstrating the consistency of the possible tumble axis directions for the same phase angle, even when observed from different stations.
- Investigate the possibility of utilizing observations from other stations to determine the direction of the tumbling axis, even when the object is located at a distance greater than 10,000 km.

We chose cylindrical rocket bodies from CZ-3B, H-2A and FALCON 9 families for quasi-simultaneous observation campaign between Faculty of Mathematics, Physics and Informatics, Comenius University in Bratislava, Slovakia and Astronomical Institute University Bern, Switzerland. We will present results of the observation campaign. These objects are on orbits with low perigees and high apogees, which makes them possible candidates for near future re-entry.

2. INSTRUMENTATION

The main instrument used in this study is 70-centimeter newtonian telescope (AGO70), located at the Astronomical and Geophysical Observatory in Modra (MPC code M34, 48.37N +17.27E). It is operated by Faculty of Mathematics, Physics and Informatics, Comenius University in Bratislava. The telescope has Newtonian design with equatorial open fork mount. System is equipped by the CCD camera FLI-ProLine PL1001 with array dimension 1024 x 1024 and rectangular pixels with size of 24μm. Effective field of view is 28.5 x 28.5 *arcmin* with pixel scale of 1.67 $arcsec/pixel$. Primary mirror has 0.7 *m* diameter and focal length is 2962 *mm*. The telescope was recently upgraded to have capability to perform the Low-Earth orbit (LEO) tracking of the orbits with mean altitude higher than 700 *km*. AGO70 is also equipped with Johnson-Cousins filters [2]. The acquired and processed data are published in Space Debris Light Curve Database (SDLCD) [3]. The telescope with in its dome is shown in Fig. 1(Left).

The second system used for the observation is Zimmerwald Laser and Astrometric Telescope (ZIMLAT), with one-metre aperture. This instrument is located at Swiss Optical Ground Station and Geodynamics Observatory (MPC code 026, 46.88N, 7.47E) in Switzeland and is operated by the Astronomical Institute of the University in Bern, Switzerland. A Ritchey-Chrétien design and an azimuth-elevation mount. It has a Nasmyth platform hosting 4 possible focusing positions with focal lengths of 1.2 *m*, 2 × 4 *m* and 8 *m*. Three of them are currently equipped with the Neo scientific CMOS tracking camera, the Spectral Instruments 1100 with a CCD sensor and a single photon counter. The scientific CCD camera is equipped by 30.7 *mm x* 31.0 *mm* with pixel size 15 μm. It is also equipped with mechanical shutter. It is mounted using the 4 *m* focal length position derotator platform, which gives a setup's field of view of 13.2 *arcmin x* 13.3 *arcmin* with the pixel scale of individual pixel is 0.387 $arcsec/pixel$. The telescope with in its dome is shown in Fig. 1 (Right).

3. ATTITUDE DETERMINATION FOR THE CYLINDRICAL BODIES

This model, assumes that a cylindrical object is significantly longer than its width and rotates around an axis perpendicular to the central axis. Theoretical calculations show that most objects of this shape are stabilized in the so-called

Fig. 1: AGO70 with its dome (left), ZIMLAT with its dome (right).

end-over-end rotation in the body-fixed reference frame. The most important relation is the Eq. 1, which expresses the apparent magnitude of a cylindrical object that reflects light only by its sides and not its ends.

$$M = -2.5 \log_{10} \left(\frac{kla\gamma F}{R^2} \right) \tag{1}$$

l in this relation is the length of the object, a is its radius, γ is albedo, F is a function of the phase angle and the orientation of the axis of rotation, R is the distance from the object to the observer and k is the solar constant.

The value F in Eq. 2 is given by the relation where $F1$ is Eq. 4 and $F2$ is Eq. 5. The $function\frac{F_1}{F_2}$ is given by Eq. 3. A is the polar angle and Γ azimuth of the central axis in the satellite coordinate system.

$$F = \frac{1}{4\pi} \left[\left(\pi - \text{function} \frac{F_1}{F_2} \right) F_2 + |F_1| \right] \tag{2}$$

where function is:

$$\text{function} \frac{F_1}{F_2} = \begin{cases} |\arctan \frac{F_1}{F_2}| & \text{if} \quad F_2 > 0 \\ \frac{\pi}{2} & \text{if} \quad F_2 = 0 \\ \pi - |\arctan \frac{F_1}{F_2}| & \text{if} \quad F_2 < 0 \end{cases} \tag{3}$$

$$F_1 = \sin\phi \sin A_a |\sin \Gamma_a| \tag{4}$$

$$F_2 = \cos^2 \frac{\phi}{2} - \sin^2 A_a . \left(\sin^2 \frac{\phi}{2} + \cos^2 \frac{\phi}{2} \cos^2 \Gamma_a \right) \tag{5}$$

where A_a and Γ_a are polar angle and azimuth angle in model's coordinate system and ϕ is phase angle.

Because debris objects can rotate very quickly (typically order of seconds up to hundreds of seconds [3]), the distance between the observer and the object does not change significantly during one rotation period. Then the change in brightness of the object during one rotation period is given by the Eq. 6.

$$M_{max} - M_{min} = -2.5 \log_{10} \left(\frac{F_{max}}{F_{min}} \right) \tag{6}$$

If the axis of rotation is perpendicular to the central axis, then a given change in brightness during one period is given by only three parameters: the phase angle, and two coordinates of the orientation of the axis of rotation. The difference

between maximum and minimum brightness is called the brightness ratio. Thus, we can use this equation to calculate the orientation of the rotation axis if we know the brightness ratio and the phase angle of the object. It is clear that there are several pairs of coordinates that will lead to a similar value of the brightness values as measured, so it is necessary to have multiple measurements at different phase angles and look for those pairs that are the solution in all cases.

3.1 Reference frames

If we want to calculate location of rotation axis, we need coordinate system which will help us to express tumbling axis orientation. Author in [1] introduced body-fixed satellite coordinate system. This system is right-handed with origin in the satellite center of mass. If s is the unit vector pointing from the satellite center of mass towards the Sun and o is the unit vector pointing from the satellite center of mass towards the observer the coordinate axes of the Williams system x, y and z are defined by Eq. 7.

$$x = \frac{s+o}{|s+o|}, \qquad y = \frac{s-o}{|s-o|} \qquad z = \frac{s \times o}{|s \times o|} \tag{7}$$

To specify the direction of a vector $\vec{v}$ in this coordinate system, we use a related spherical coordinate system with the polar angle A and the azimuth angle Γ. The polar angle is between the z-axis and $\vec{v}$, taking values from 0 to π, and the azimuth angle is between the x-axis and the projection of $\vec{v}$ onto the x-y-plane, taking values from 0 to 2π. The conversion from a unit vector v to A and Γ is given by Eq. 8, while the backwards conversion is given by Eq. 9. This is shown in Fig. 2 [1].

$$\Gamma = \arctan\left(\frac{v_y}{v_x}\right), \qquad A = \arccos(v_z) \tag{8}$$

$$\begin{aligned} v_x &= \sin(A)\cos(\Gamma) \\ v_y &= \sin(A)\sin(\Gamma) \\ v_z &= \cos(A) \end{aligned} \tag{9}$$

We will present our results in Equatorial coordinate system which has origin in the center of the Earth and the J2000 as a reference frame. This frame has x-axis towards the Sun at the spring equinox, z-axis along the Earth's polar axis and y-axis completing the right-handed set.

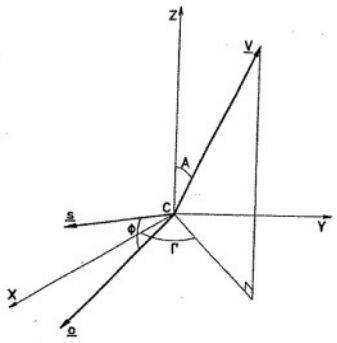

Fig. 2: The body-fixed coordinate system as defined in the original William's model for the attitude determination of the cylindrical body [1].

3.2 Model assumptions

The object and its motion must meet several conditions in order for Williams approach to be applicable and as realistic as possible. Still, it will only be an approximation of real conditions. Most of all, the object must be inactive, that is, its attitude must not be artificially altered, especially the speed of its rotation and its orientation in space.

The light curve of the object must show significant changes, i.e. there must be regular maxima and minima in it. This is due to the fact that the object must rotate with a certain period. Stable and chaotically rotating objects do not have a stable light curve and consequently a phase diagram with a precisely determined amplitude.

Another strong requirement is on the shape of the object. The model assumes a cylindrical object with several times greater length than its width. Such dimensions ensure end-over-end rotation. The ends of the object must reflect as little light as possible. This requirement is met by rocket bodies, as their lower part is formed by a nozzle, which is usually dark in colour and both upper stage's bases has significantly smaller area in comparison to its coat [2].

Object observations must be done in at least two different times with not too long temporal separation, to be able to resolve as fast changes in the tumbling axis orientation as possible. Therefore, if the solution exists, it means that the orientation of the tumbling axis was stable during data acquisition, i.e. the tumbling axis is not undergoing rapid nutation or precession. It is possible that the orientation of the tumbling axis will change rapidly also due to the natural effects. That is the main reason why we decided to observe simultaneously from two different sensors and increase the data acquisition effectively.

3.3 Our implementation

Attitude determination script is Python script for computing location of the rotation axis of a cylindrical objects. The basic input parameters of Attitude determination script are: observed brightness ratio, error in the observed brightness ratio σ and mutual geometry between observer, object and the Sun obtained from orbital elements valid for the closest date to observation dates [4].

Brightness ratio and its error are extracted through the routine for the light curve processing developed in Faculty of Mathematics, Physics and Informatics, Comenius University in Bratislava [3]. This routine is suitable also for ZIMLAT data.

Phase angle, vector from the object to the Sun and from the object to observer are computed from observer, object and the Sun position vector in geocentric celestial reference system. The script iterates through the values of A and Γ and computes brightness ratio for each pair of A and Γ, where A is the polar angle and Γ is the azimuth angle in the object polar coordinate system [1]. Then script generates colour map of brightness ratios. In the next step, coordinates of brightness ratio within $\pm\sigma$ of the observed value are extracted and shown in graph with axis A_t and Γ_t, where t means tumble axis. Extracted coordinates are possible directions of tumbling axis for the specific phase angle. The brightness ratio is computed for every phase angles under which the observation was done. If the observations only from one location are provided, then the observation must be done on three different observation times. The greater number of the observations, the more accurate the calculation is. If the brightness ratio is computed for every phase angle, then values A and Γ are transform in J2000 coordinate system. Finally, the intersection points of location of possible tumbling axis orientation for all observed phase angles are calculated and shown in 2D graph. The intersection points are the most possible directions of the tumbling axis.

4. RESULTS

In this section, we present the preliminary campaign results and the calculation of the orientation of the tumble axis for the selected objects. We initiated the campaign by observing CZ-3B rocket bodies and subsequently shifted our focus to H-2A rocket bodies. This change was caused by the presence of the specular flashes, which can be used for attitude determination by different independent method. For the processing using [1], the specular flashes were removed from the light curves, aligning with the model's assumption of only diffuse reflection. The need to remove specular flashes also applies to the FALCON 9 rocket body. These light curves are shown in Fig. 4. All target objects are on geotransfer orbit (GTO) characterized by a low perigee and high apogee. The target objects are shown in Fig. 3. We use amplitude error with value 10% of observed amplitude.

Fig. 3: Target objects: H-2A (left)[5]; Falcon 9 (middle)[6] and CZ-3B (right)[7].

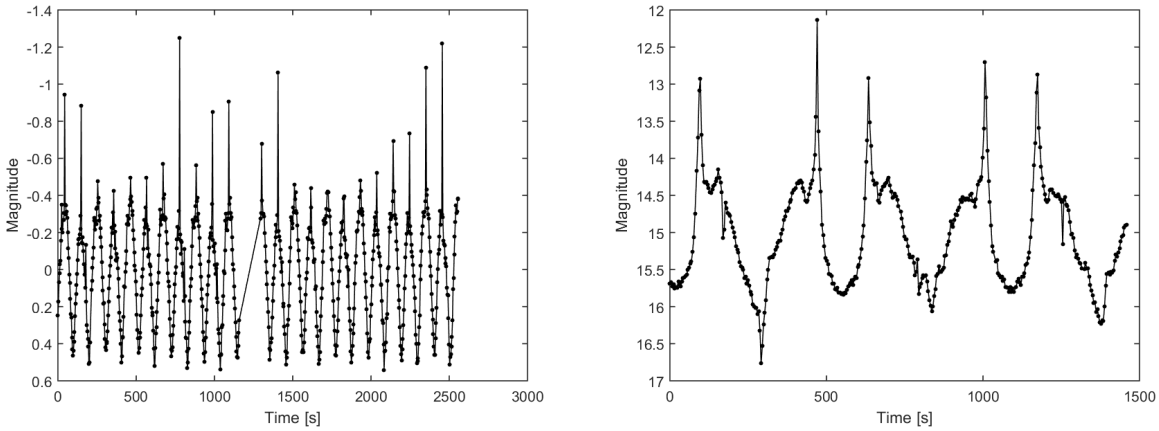

Fig. 4: Light curve of Falcon 9 with specular flashes measured in instrumental magnitudes (left), light curve of H-2A with specular flashes measured in standard magnitudes (right).

4.1 CZ-3B - NORAD 43624, COSPAR 2018-072C

The rocket body NORAD 43624, COSPAR 2018-072C, belongs to the CZ-3B type. It was launched on September 19, 2018. Details regarding the observation times and the distances of the target object from the observer during these observations are presented in Tab. 1. Using these observations, we performed calculations to determine the orientation of the tumble axis. The outcomes are visualized in Fig. 5.

There are two regions of possible solutions: $DEC = -3°$, $RA = 65°$, and $DEC = 39°$, $RA = 145°$. There are two additional regions with opposing directions. This ambiguity is likely attributable to extended intervals between observations, considering that the object was in a geotransfer orbit (GTO) featuring a perigee approximately 200 *km* above Earth's surface. The passage through the perigee might have caused changes in the rotation axis. The range of the phase angle was only 28 *degrees*, which might be insufficient to find only one region of possible solutions. The object is no longer on orbit.

Sensor	Series Start (UTC)	Distanstance [km]	Phase Angle [deg]
AGO70	21:00:27, February 7, 2023 (UTC)	14,062	74
ZIMLAT	21:31:32, February 7, 2023 (UTC)	16,139	67
ZIMLAT	21:01:30, February 9, 2023 (UTC)	10,923	95

Table 1: Acquired observation data for NORAD 43624, COSPAR 2018-072C, CZ-3B upper stage from two different sensors.

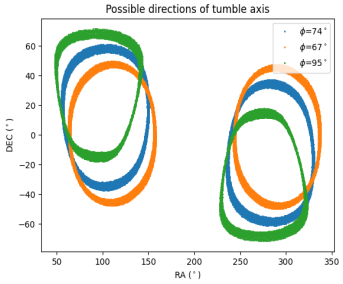

Fig. 5: Possible tumble axis directions of NORAD 43624, COSPAR 2018-072C, CZ-3B upper stage in Equatorial coordinates at J2000 epoch.

4.2 CZ-3B - NORAD 44796, COSPAR 2019-078D

The object NORAD 44796, COSPAR 2019-078D is also a CZ-3B type rocket body in GTO. The times and distances from observing this object during the campaign are listed in Tab. 2. In this case, each observation was necessary. By ignoring any of them, we obtain multiple solutions. Based on the presented calculations, we can say that the object rotated around an axis perpendicular to the central axis of the object during observations. The tumble axis had approximate coordinates: $DEC = -29^{\circ}$, $RA = 130^{\circ}$. The outcomes are visualized in Fig. 6.

Sensor	Series Start (UTC)	Distanstance [km]	Phase Angle [deg]
ZIMLAT	03:17:32, February 7, 2023 (UTC)	6,252	27
ZIMLAT	21:07:31, February 7, 2023 (UTC)	19,092	92
AGO70	23:50:36, February 8, 2023 (UTC)	12,321	59
AGO70	00:00:13, February 9, 2023 (UTC)	10,445	54

Table 2: Acquired observation data for NORAD 44796, COSPAR 2019-078D, CZ-3B upper stage from two different sensors.

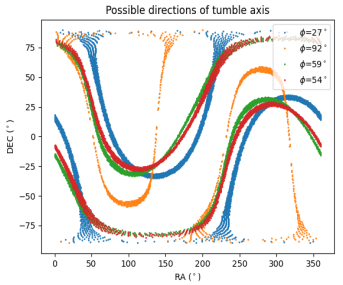

Fig. 6: Possible tumble axis directions of NORAD 44796, COSPAR 2019-078D, CZ-3B upper stage in Equatorial coordinates at J2000 epoch.

4.3 H-2A - NORAD 26899, COSPAR 2001-038B

For the object NORAD 26899, COSPAR 2001-038B, we had enough observations to calculate the orientation of the tumble axis for two days: May 27 and June 1, as shown in Tab. 3. This object is the H-2A rocket body in GTO. For the calculations using the observations from May 27 shown in Fig. 7, two regions emerge: $DEC = 7°$, $RA = 35°$ and $DEC = 48°$, $RA = 57°$. The second region would likely disappear when using a smaller amplitude error. Each of these regions also has an opposing solution. For the solutions from June 1, it is similar. Two possible regions are: $DEC = -2°$, $RA = 38°$ and $DEC = 50°$, $RA = 86°$, with corresponding opposing solutions. Considering only the first mentioned solutions, it can be stated that the object's orientation changed by 9° in declination and 3° in right ascension. The two observations from June 1 have the same phase angle, but the potential solutions for these phase angles are not the same.

Sensor	Series Start (UTC)	Distanstance [km]	Phase Angle [deg]
ZIMLAT	21:27:40, May 27, 2023 (UTC)	24,305	8
AGO70	22:40:17, May 27, 2023 (UTC)	30,805	25
AGO70	23:40:03, May 27, 2023 (UTC)	33,326	35
AGO70	01:35:18, May 28, 2023 (UTC)	31,513	53
ZIMLAT	23:14:27, June 1, 2023 (UTC)	20,392	14
AGO70	00:00:33, June 2, 2023 (UTC)	26,431	14
AGO70	00:58:49, June 2, 2023 (UTC)	31,264	24

Table 3: Acquired observation data for NORAD 26899, COSPAR 2001-038B, H-2A upper stage from two different sensors.

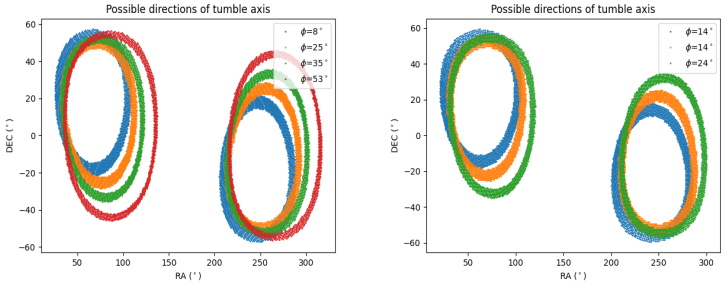

Fig. 7: Left: Possible tumble axis directions of NORAD 26899, COSPAR 2001-038B, H-2A upper stage in Equatorial coordinates at J2000 epoch using observations from May 27, 2023. Right: Possible tumble axis directions of NORAD 26899, COSPAR 2001-038B, H-2A upper stage in Equatorial coordinates at J2000 epoch using observations from June 1, 2023.

4.4 H-2A - NORAD 28938, COSPAR 2006-004B

The object NORAD 28938, COSPAR 2006-004B, is an H-2A rocket body in GTO. The observations were conducted over the course of several hours as can be seen in Tab. 4. When using observations from just one sensor, multiple possible solutions were revealed. When combined, the most reliable solution appears to be with coordinates: $DEC = -59°$, $RA = 177°$, along with its opposing solution, shown in Fig. 8. Unlike the previous case where the possible solutions for the same phase angles did not match, in this instance, the solutions for phase angles 34° and 29° are nearly identical. The object was passing through the apogee during the observation.

Sensor	Series Start (UTC)	Distanstance [km]	Phase Angle [deg]
AGO70	22:25:13, April 25, 2023 (UTC)	20,159	69
ZIMLAT	23:00:59, April 25, 2023 (UTC)	24,361	56
AGO70	00:40:03, April 26, 2023 (UTC)	30,276	34
ZIMLAT	01:07:03, April 26, 2023 (UTC)	30,531	29
ZIMLAT	02:39:49, April 26, 2023 (UTC)	26,199	11

Table 4: Acquired observation data for NORAD 28938, COSPAR 2006-004B, H-2A upper stage from two different sensors.

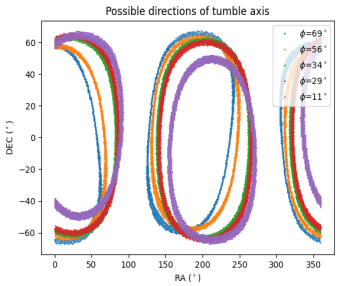

Fig. 8: Possible tumble axis directions of NORAD 28938, COSPAR 2006-004B, H-2A upper stage in Equatorial coordinates at J2000.

4.5 H-2A - NORAD 37159, COSPAR 2010-045B

The object NORAD 37159, COSPAR 2010-045B is an H-2A rocket body on GTO. For this object, we have only one observation from AGO70 and one from ZIMLAT, shown in Tab. 5, which was insufficient to find a solution, as depicted in Fig. 9. There were several such cases during the campaign, either due to limited observations of the objects or with significant time gaps. This occurred primarily due to weather conditions.

Sensor	Series Start (UTC)	Distanstance [km]	Phase Angle [deg]
ZIMLAT	21:31:44, May 26, 2023 (UTC)	10,535	27
AGO70	00:56:40, May 27, 2023 (UTC)	9,836	18

Table 5: Acquired observation data for NORAD 37159, COSPAR 2010-045B, H-2A upper stage from two different sensors.

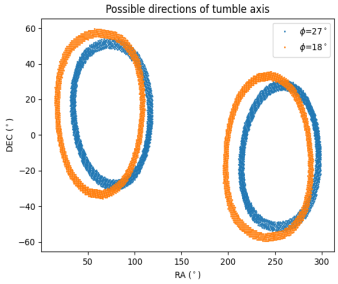

Fig. 9: Possible tumble axis directions of NORAD 37159, COSPAR 2010-045B, H-2A upper stage in Equatorial coordinates at J2000.

4.6 FALCON 9 - NORAD 54248, COSPAR 2022-153C

The object NORAD 54248, COSPAR 2022-153C is the only FALCON 9 rocket body. It is on an orbit with a perigee of around 200 *km* and an apogee of about 58,000 *km*. The object was observed over a period of three hours, as shown in Tab. 6. A specific solution could not be found, as depicted in Fig. 10. The solution region is relatively distinct in right ascension but widely dispersed in declination. This object may not be in the simple rotation we assume, given that it was launched on November 12, 2022, and due to its low perigee, it is under influence of torques. Remarkably, specular flashes were observed for this object. The solutions in Fig. 11 are for observations that were made from both stations at the same time. They are nearly identical and have the same phase angle.

Sensor	Series Start (UTC)	Distanstance [km]	Phase Angle [deg]
AGO70	20:12:32, June 1, 2023	41,896	83
ZIMLAT	20:54:03, June 1, 2023	36,652	79
AGO70	22:28:43, June 1, 2023	21,834	61
AGO70	22:56:17, June 1, 2023	15,730	48

Table 6: Acquired observation data for NORAD 54248, COSPAR 2022-153C, FALCON 9 upper stage from two different sensors.

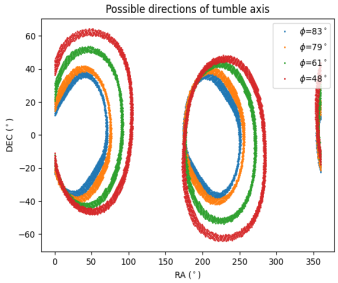

Fig. 10: Possible tumble axis directions of NORAD 54248, COSPAR 2022-153C, FALCON 9 upper stage in Equatorial coordinates at J2000.

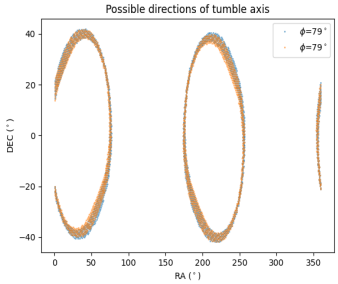

Fig. 11: Possible tumble axis directions of NORAD 54248, COSPAR 2022-153C, FALCON 9 upper stage in Equatorial coordinates at J2000 when object was observed in the same time from both stations. Object was in distance 36,650 *km*.

5. CONCLUSIONS AND FUTURE WORK

In this paper, we presented the results of a observational campaign between the Faculty of Mathematics, Physics, and Informatics at Comenius University in Bratislava, Slovakia, and the Astronomical Institute of the University of Bern, Switzerland. The observations were conducted using the AGO70 and ZIMLAT telescopes. The campaign ran from the end of 2022 to the end of June 2023. Our focus was on cylindrical objects in GTO orbits, specifically rocket bodies of the following types: CZ-3B, H-2A, and FALCON 9. Objects on these orbits will re-enter the atmosphere in the near future. Furthermore, rocket bodies are candidates for ADR missions due to their significant dimensions. For an ADR mission, it is crucial to have a comprehensive understanding of the rotational characteristics of the target object. The objective was to utilize these observations to calculate the orientation of the tumble axis of the observed objects. Furthermore, we aimed to explore how observations from two different stations can contribute to this calculation.

To calculate the orientation of the tumble axis, we used the low-resolution Williams method [1], which is applicable to cylindrical objects in tumbling motion — rotation around an axis perpendicular to the object's central axis. For the utilization of this method, it is necessary to observe the object at various phase angles. However, the time elapsed between observations should be kept as short as possible to be able to resolve also rapid changes in the tumble axis due to natural torques. The more observations taken at different phase angles, the more definitive the solution becomes. For an object to be suitable for this method, its cylindrical coat must dominate its structure, and the ends should reflect minimal light.

For object NORAD 44796, COSPAR 2019-078D, CZ-3B upper stage, the solution for the orientation of the rotational axis was unambiguous. This would indicate that this object was in tumbling motion at the time of observation, with a tumbling axis having specific coordinates. This object has already decayed and is no longer in orbit. For object NORAD 28938, COSPAR 2006-004B, H-2A upper stage, the solution was unique, but additional possible solution regions were also identified. In both cases, observations from both instruments were helpful. Using observations from only one sensor would have resulted in a highly ambiguous solution. In the case of NORAD 26899, COSPAR 2001-038B, H-2A upper stage, it became evident that the solution depends not only on the phase angle. Even when observed at the same phase angle, the possible orientation regions differed. This means that observations with the same phase angle can be used in the solution if that phase angle occurred at a different time. For the last presented object NORAD 54248, COSPAR 2022-153C, FALCON 9 upper stage, it was shown that when observed at the same time, even if the object is too distant ($35,000\ km$), the area of possible solutions remains the same. This indicates that if an object is sufficiently distant, it's unnecessary to observe it simultaneously with two sensors. These findings can aid in planning future observations.

During the campaign, a significant number of specular flashes were observed for objects of the H-2A type. These specular flashes were captured with varying intensity and at different moments at both observation stations. With a good understanding of the shape of the H-2A object, these observations can be used to calculate the orientation of the tumbling axis by independent method, which can serve us as a cross-validation of both approaches. Specular flashes were also observed for the object NORAD 54248, COSPAR 2022-153C, FALCON 9 upper stage. The future work will be oriented on the further campaign observation and implementation of the attitude determination based on the specular flashes, which can be usable for also different shapes as a cylindrical bodies.

6. REFERENCES

[1] V. Williams. Location of the rotation axis of a tumbling cylindrical earth satellite by using visual observations: Part i: Theory. *Planetary and Space Science*, 27(6):885–890, 1979.

[2] M. Zigo, J. Šilha, Hrobár T., and P Jevčák. Space debris surface characterization through BVRcIc photometry [inpress]. *Advances in Space Research*, 2023.

[3] Šilha J. et al. Space debris observations with the Slovak AGO70 telescope: Astrometry and light curves. *Advances in Space Research*, 65(8):2018–2035, 2020.

[4] USSTRATCOM. SpaceTrack. `https://www.space-track.org/documentation#/faq`. Online; Accessed: 07.01.2020.

[5] P. Blau. Japanese h-iia rocket fires into orbit with climate change satellite amp; super-low altitude testbed. `https://spaceflight101.com/h-iia-gcom-c1/h-iia-launches-gcom-c-and-slats/`, Dec 2017.

[6] SpaceX. Falcon 9. `https://www.spacex.com/vehicles/falcon-9/`, 2023.

[7] Shangai Academy for Spaceflight Technology. 300 launches! a milestone of long march series launch vehicle, and a new beginning of china aerospace. https://www.sast.net/news/63.html, Mar 2019.